Direct Electrodeposition of Graphene–Gold Nanocomposite Films for Ultrasensitive Voltammetric Determination of Mercury(II)

ARTICLE *in* ELECTROANALYSIS · JANUARY 2014

Impact Factor: 2.14 · DOI: 10.1002/elan.201300226

5 AUTHORS, INCLUDING:

Liang Ding
Jiangsu Provincial Academy of Environmen…
16 PUBLICATIONS **140** CITATIONS
SEE PROFILE

Yuping Liu
Monash University (Australia)
17 PUBLICATIONS **106** CITATIONS
SEE PROFILE

Jie Zhang
Monash University (Australia)
67 PUBLICATIONS **1,134** CITATIONS
SEE PROFILE

DOI: 10.1002/elan.201300226

Direct Electrodeposition of Graphene-Gold Nanocomposite Films for Ultrasensitive Voltammetric Determination of Mercury(II)

Liang Ding,[a, b] Yuping Liu,[a] Jianping Zhai,[b] Alan M. Bond,*[a] and Jie Zhang*[a]

Abstract: Graphene-gold nanocomposite (rGO-Au) modified glassy carbon electrodes (GCE) have been fabricated by a one-step electrodeposition method. The nanocomposites were characterized by scanning electron microscopy, energy dispersive X-ray spectroscopy, Raman spectra as well as electrochemical methods, and were utilized for mercury(II) detection via anodic stripping voltammetry. The peak stripping current was linearly dependent on the concentration of Hg(II) over the range of 1.0 to 150.0 nM and high selectivity and sensitivity (limit of detection 0.6 nM) and excellent stability/reusability were achieved. The applicability to environmental samples was successfully demonstrated by the direct determination of Hg(II) in tap water samples with minimal sample pretreatment.

Keywords: Graphene-gold composite electrodes · Electrodeposition · Mercury(II) detection · Anodic stripping analysis

1 Introduction

Mercury, mainly from modern industrial processes, is considered to be a highly toxic heavy metal [1]. Hg(II) is highly dangerous even at a very low concentration level [2]. High exposure may result in kidney and respiratory failure and damage to the gastrointestinal tract and nervous system [3]. The guideline value set by the World Health Organization (WHO) for Hg(II) in drinking water is 1 $\mu g L^{-1}$ (5 nM), which is applied in many countries [4]. Consequently, there is a need for the development of rapid determination and reliable methods of quantification of trace levels of mercury in the environment for public security and health protection.

A variety of spectroscopic techniques have been employed for Hg(II) trace determination with excellent selectivity and sensitivity. These include atomic absorption spectrometry (AAS) [5,6], atomic fluorescence spectroscopy (AFS) [7,8], ion coupled plasma mass spectrometry (ICPMS) [9,10] and microwave induced plasma atomic emission spectroscopy (MIP-AES) [11]. However, they are all limited with respect to in situ or on line and automated analysis. Low-cost electrochemical methods, particularly anodic stripping voltammetry (ASV), do not have these restrictions and thus have attracted significant interest for their excellent sensitivity and suitability for field-based analysis [12–16]. Gold has been found to be the best electrode material for the determination of mercury. Gold has a high affinity for mercury, which enhances the preconcentration effect. However, amalgam formation causes a structural change to the gold electrode surface and time-consuming cleaning treatments are needed to achieve reproducibility. In recent years, nanotechnology has become one of the most active areas of research in analytical chemistry. Of interest to this work, gold nanoparticles (AuNPs) based sensors have been extensively investigated for electroanalysis of Hg(II), demonstrating that AuNPs-based nanocomposites combined with ASV could be satisfactory for Hg(II) detection [17–21]. In our previous research, a poly(hydroxymethyl 3,4-ethylenedioxythiophene) stabilized Au nanoparticle modified glassy carbon electrode was successfully fabricated as a reusable sensor for mercury(II) detection at micromolar concentration levels [22]. Nevertheless, it is still a great challenge to homogenously distribute monodispersed AuNPs on the supporting skeleton for monitoring of Hg(II).

Graphene, a 2D sp^2-hybridized carbon sheet, also has attracted much attention due to its unique electrical, thermal, optical, and mechanical properties as well as its potential use in various fields, such as nanoelectronic devices, sensors, solar cells, and composite materials [23–28]. Recently, graphene-based gold nanocomposites (Gr-Au) have been developed as an advanced nanoelectrocatalyst for constructing Hg(II) sensors [3,29,30]. Generally, two steps are involved in the fabrication of Gr-Au: (i) modification of graphene on the substrate and (ii) deposition of AuNPs on the graphene film. The commonly adopted drop-casting method for preparation of electrodes usually results in a non-uniform coating of the Gr thin film onto the electrode and does not allow good control over the

[a] L. Ding, Y. Liu, A. M. Bond, J. Zhang
School of Chemistry, Monash University, Clayton, Victoria, 3800, Australia
*e-mail: alan.bond@monash.edu
jie.zhang@monash.edu

[b] L. Ding, J. Zhai
State Key Laboratory of Pollution Control and Resource Reuse, School of the Environment, Nanjing University, Nanjing 210093, P. R. China

film thickness. In this paper, fabrication of Gr-Au nanocomposite is achieved homogeneously and directly in the construction of a Hg(II) sensor.

Finally, it is noted that the use of chemical and thermal methods involving highly toxic chemicals is a health hazard and time consuming. Thus Liu [31] explored a new and simple method to prepare graphene-metal nanocomposite by one-step electrochemical deposition. Herein, the reduced graphene oxide-gold nanocomposite film (rGO-Au) is directly and homogeneously deposited on a glassy carbon electrode (GCE) by one-step electrodeposition, which is a safe method of sensor preparation. The nanocomposite film was characterized by cyclic voltammetry (CV), scanning electron microscopy (SEM), energy dispersive X-ray spectroscopy (EDX) and Raman spectra. The performance of rGO-Au for Hg(II) detection was investigated by means of dc anodic stripping voltammetry. The platform was also successfully applied for trace Hg(II) determination in tap water.

2 Experimental

2.1 Chemicals

Chemicals used in this work, including Na_2CO_3, $NaHCO_3$, $HAuCl_4 \cdot 3H_2O$ and $HgCl_2$, are all of analytical-reagent grade, purchased from Aldrich and used as received. Hg^{2+} solutions were prepared by diluting an appropriate amount of stock solution containing 100.0 μM Hg^{2+} ($HgCl_2$). All aqueous solutions were prepared using distilled water.

2.2 Apparatus

Electrochemical measurements were performed at 25 °C with a BAS 100B electrochemical workstation (Bioanalytical Systems Inc., USA) using a conventional three-electrode cell comprising a platinum wire counter electrode, a Ag/AgCl (3 M KCl) reference electrode and modified or unmodified glassy carbon electrode (GCE, 3 mm in diameter, CH Instruments, USA) working electrodes. Prior to use, the GCE was polished to a mirror finish using alumina slurries and successively sonicated in ethanol and distilled water for 2 min. Finally, it was rinsed thoroughly with distilled water and dried under ambient temperature.

The general morphology and chemical composition of the electrodeposited films were characterized by scanning electron microscopy (SEM) and energy dispersive X-ray spectroscopy (EDX) on JEOL 7001F FEG Instrument. Raman spectra were obtained using a Renishaw inVia Microscope.

2.3 Fabrication of the Modified Electrode

Graphite oxide was synthesized from graphite by the Hummers method [32]. The synthesized graphite oxide powder was exfoliated in a 0.1 M pH 9.0 carbonate buffer solution (CBS) by ultrasonication for 1 h to form a 1.0 mg mL^{-1} GO colloidal dispersion. The appropriate amount of tetrachloroauric acid was then added into the GO solution, and cyclic voltammetric reduction was performed from the deposition solution with magnetic stirring using a similar procedure to that described in our previous paper [33]. Several cycles of potential were performed over the range of −1.5 and 0.6 V at a scan rate of 25 mV s^{-1}. The composite loading was controlled by the number of cycles (N). After electrodeposition, the reduced graphene oxide-gold modified GCE (rGO-Au/GCE) was thoroughly rinsed with distilled water and then kept under ambient conditions prior to use. For comparison, rGO was electrodeposited on GCE in 0.1 M pH 9.0 CBS with 1.0 mg mL^{-1} GO.

2.4 Stripping Voltammetric Detection of Hg(II)

The electrochemical assay of Hg(II) on rGO-Au/GCE is illustrated in Figure 1. Firstly, mercury (Hg(0)) is deposited from Hg(II) at 0.3 V for 600 s in 0.01 M HCl under magnetic stirring. Then, anodic stripping of Hg(0) is performed by scanning the potential from 0.2 to 0.8 V at a scan rate of 250 mV s^{-1}. After multiple cycles of potential, the deposited mercury could be removed to regener-

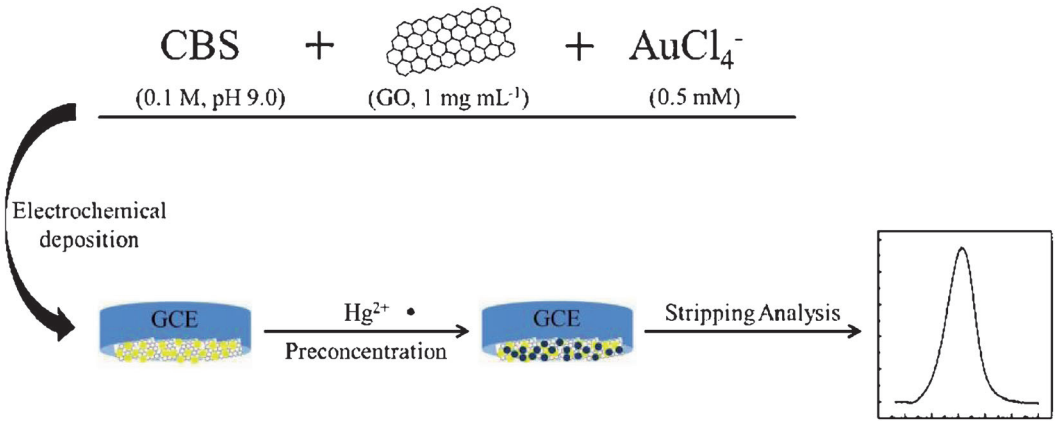

Fig. 1. Electrochemical assay of Hg(II) on a rGO-Au/GCE.

ate the electrode surface. Data achieved from multiple cycles of potential without a stripping signal was considered to be the blank. Hg stripping currents were measured from results obtained after subtraction of this blank. This procedure, known as the "subtractive method", is similar to ones reported in the literature [20,21] and enables the analytical results to be free of background vagaries. An acidic medium is chosen for Hg analysis to prevent the hydrolysis of Hg^{2+}.

3 Results and Discussion

3.1 Electrodeposition of rGO-Au on GCE

Figure 2 displays cyclic voltammograms for the electrodeposition of reduced graphene oxide (a, rGO) and reduced graphene oxide-gold (b, rGO-Au) on GCE for 4 cycles of potential. As can be seen from Figure 2a, the reduction peak I at −1.3 V is assigned to the irreversible electrochemical reduction of GO [34] and the persistent increase of peak current with each cycle confirms the reduction of GO to rGO has been achieved on the surface of the GCE. Anodic peak II and cathodic peak III are attributed to the redox pair of oxygen functional groups on the graphene plane [31]. After the addition of $AuCl_4^-$ into the electrolyte, the cyclic voltammograms (Figure 2b) display a distinct difference from that for GO deposition. Clearly, the reduction currents, involving the reduction of $AuCl_4^-$, are dramatically larger than those for the GO reduction. The cathodic peak and the continuous increasing current with potential cycling verify the persistent and simultaneous deposition of rGO and Au on the GCE.

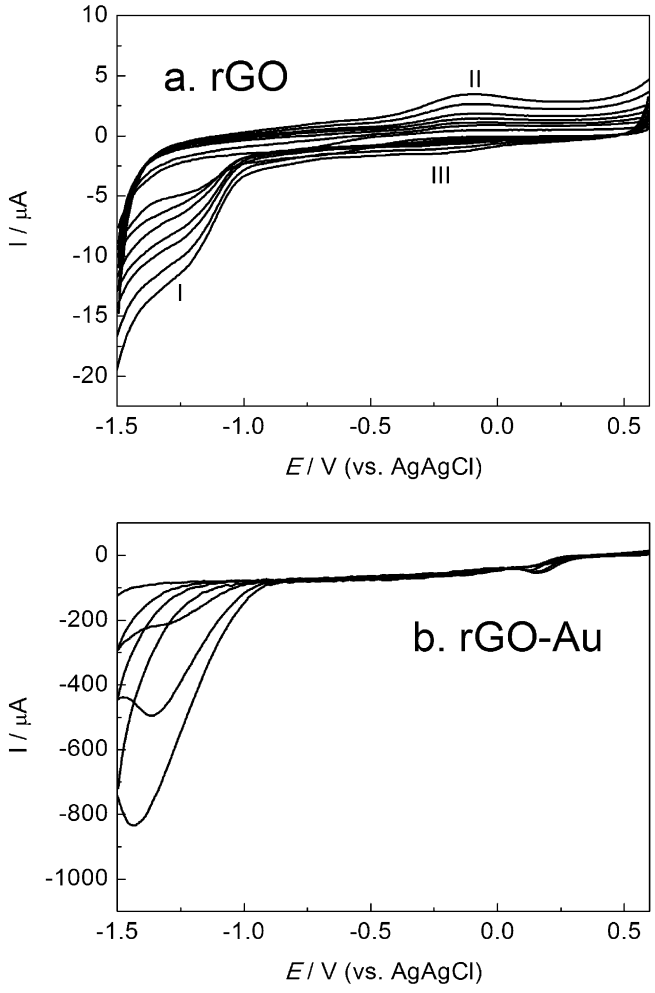

Fig. 2. Cyclic voltammograms at a GCE for the electrolysis of a magnetically stirred solution (a) 1.0 mg mL^{-1} GO and (b) 1.0 mg mL^{-1} GO + 0.5 mM $AuCl_4^-$ in pH 9.0 CBS at a scan rate of 25 mV s^{-1}.

3.2 Characterization of rGO-Au

Figure 3a presents the cyclic voltammograms of GCE, rGO/GCE and rGO-Au/GCE in 1.0 M KCl. As expected, the background current for GCE, rGO/GCE ($N=1$) and rGO-Au/GCE ($N=1$) steadily increase with increasing surface area of the GCE via rGO deposition and simultaneous incorporation of AuNPs. Meanwhile, the background current for rGO/GCE ($N=5$) is higher than rGO/GCE ($N=1$), indicating that rGO is continuously electrodeposited on GCE. Further characterization of rGO-Au/GCE ($N=1$) was carried out in a 0.5 mol L^{-1} H_2SO_4 solution. As shown in Figure 3b, the voltammetric behavior exhibited typical characteristics of Au, with two oxidation peaks at 1.18 and 1.36 V corresponding to the formation of Au oxides. A reduction peak at 0.93 V is a result of the reduction of a Au oxide. These data confirm the formation of the rGO-Au nanocomposite on GCE.

Figure 4a, b and c illustrate the SEM images of the different modified electrodes obtained by electrodeposition. Figure 4a reveals a wrinkled texture associated with the presence of flexible graphene sheets. The rGO, which was electrodeposited on GCE, clearly shows the flake-like shape. Figure 4b is the SEM image of the prepared rGO-Au nanocomposite, indicating rGO-Au could be synthesized in a one pot electrochemical method. The rGO-Au image (inset) clearly suggests a homogeneous distribution of discrete gold nanoparticles on the graphene surface and the well-packed graphene films. The AuNPs evenly distributed on a rGO sheet may provide a large available surface area and enhance the electrochemical activity [35]. For comparison, the SEM image of rGO-Au/GCE after ten successive cycles of Hg(II) accumulation and stripping is presented in Figure 4c. There is no obvious difference between the original and cycled ones, indicating that the amalgam formation between Hg(0) and Au NPs did not result in any morphology change. From this point of view, rGO-Au/GCE could be considered as a reusable Hg(II) sensor. EDX was also employed to determine the chemical composition of the electrodeposited film. As shown in Figure 4d, the EDX data obtained from rGO-Au film shows the well characterized peaks arising from Au from Au NPs and C from rGO, as expected.

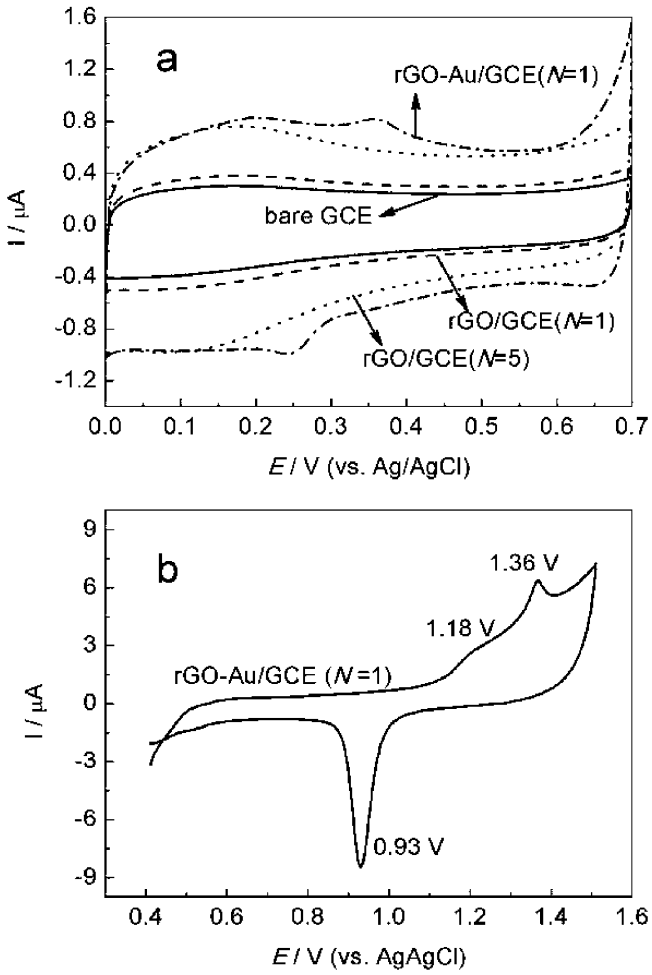

Fig. 3. Cyclic voltammograms for bare GCE, rGO/GCE and rGO-Au/GCE in (a) 1.0 M KCl and (b) 0.5 M H_2SO_4 at a scan rate of 20 mV s^{-1}.

Raman spectroscopy was used to characterize the structural changes of graphene-based materials, including disorder and defect structures [36]. The Raman spectra of GO, rGO and rGO-Au are shown in Figure 4e. Two bands, observed at 1370 and 1601 cm^{-1} are ascribed to the D band (symmetrical A_{1g} mode) and the G band (E_{2g} mode of sp^2 carbon atoms), respectively [37,38]. It is well known that changes in the relative intensities of the D and G bands (D/G) indicate changes in the electronic conjugation state of the GO during reduction. Compared to that in GO, the D/G intensity ratio increased after electrochemical reduction, suggesting that smaller sp^2 domains are formed upon reduction of the exfoliated GO [39]. This observation also verifies that the electrochemical reduction of GO has indeed taken place.

3.3 Electrochemical Response of Hg(II) at rGO-Au/GCE

The electrochemical response of Hg(II) at a rGO-Au/GCE was investigated via scanning the potential from 0.2 to 0.8 V at a rate of 250 mV s^{-1}. Figure 5a provides a voltammogram at the rGO-Au/GCE ($N=1$), when preconcentration was carried out for 600 s at 0.3 V in a 0.01 M HCl solution containing 100.0 nM Hg(II). Three well-defined oxidation processes are observed. Process I (peak potential = 0.38 V) was also observed previously at an Au nanoparticle modified electrode in a similar electrolyte medium and was assigned to the formation of an adlayer of Cl^- anions on the Au surface [40]. The Process II (peak potential = 0.55 V) was not observed at rGO/GCE. Therefore, it is an Au related process, although the full details of the mechanism are unknown. Process III (peak potential = 0.65 V), which was not observed in the absence of Hg(II), corresponds to the stripping of mercury. This process was not observed at either bare GCE or rGO/GCE under the same experimental conditions confirming the important role of Au in the preconcentration of Hg. After multiple scanning of the potential, the stripping signal disappeared and the data obtained was used as the analytical blank for background subtraction. The resulting signal obtained after background subtraction is depicted in the Inset of Figure 5a and was used for the analytical determination of Hg(II).

3.4 Optimization of Experimental Parameters

In order to achieve optimal performance for Hg(II) detection on a rGO-Au/GCE, parameters including number of deposition cycles of rGO-Au (N), scan rate for Hg(0) stripping, deposition potential as well as deposition time were all optimized in a 0.01 M HCl solution containing 100.0 nM Hg(II).

Figure 5b and c show the subtracted peak current (ΔI_p) corresponding to Hg reoxidation as a function of N and scan rate. It can be seen that the rGO-Au/GCEs with different deposition scans achieve similar ΔI_p values. The only difference is that the background current increases on increasing the number of cycles for rGO-Au deposition (not shown here). This is different from results reported with other AuNPs constructed Hg(II) sensors where the performance for mercury detection is associated with the number of gold deposition cycles [3,20,21]. In the present situation, the amount of deposited rGO and Au for each cycle is equal and only the outermost layer of rGO-Au nanocomposite acts as the sensor for Hg(II) detection. The influence of scan rate (v) on ΔI_p was studied over the range of 10 to 350 mV s^{-1} (Figure 5c). Cleary, ΔI_p increased upon increasing the scan rate in line with the equation $y = 0.033x + 0.895$ ($R^2 = 0.984$). This linear relationship implies that thin layer process dominates in the timescale of the voltammetric experiments [41]. Here, $v = 250$ mV s^{-1} was chosen as the scan rate for mercury stripping.

Figure 5d shows the effect of deposition potential on ΔI_p. ΔI_p increases on decreasing the deposition potential from to 0.5 to 0 V. Generally, negative potentials favor accumulation of Hg(II). However, a further decrease in the deposition potential to more negative values led to a slight decline in peak current due to the competitive

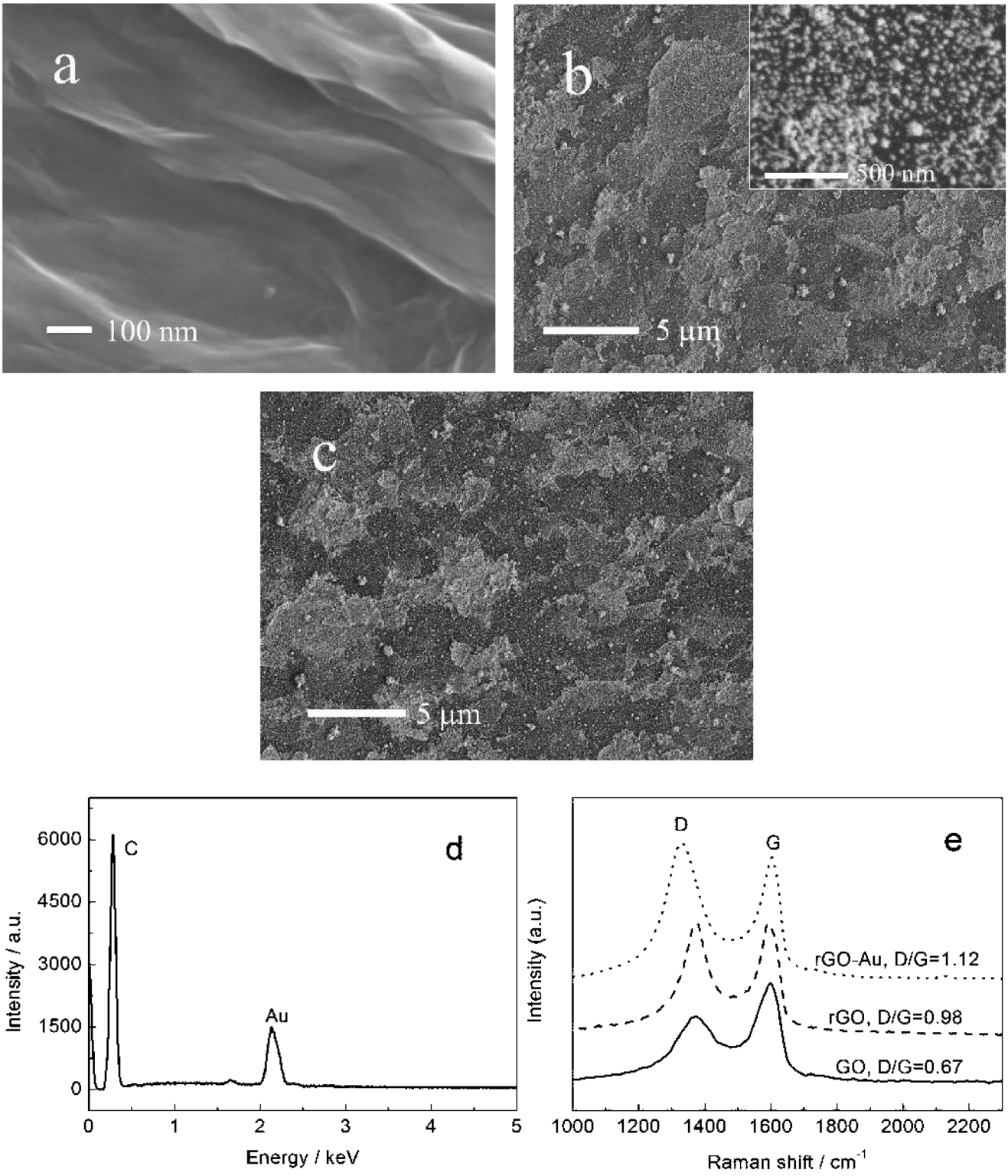

Fig. 4. SEM images of (a) rGO, (b) rGO-Au nanocomposite film. Inset: enlarged SEM image. (c) rGO-Au film after ten successive Hg(II) accumulation and stripping process; (d) EDX of the rGO-Au; (e) Raman spectra of GO, rGO and rGO-Au.

generation of H_2 [42]. Therefore, 0.3 V was chosen as the deposition potential in this study. Figure 5e shows the dependence of stripping response on deposition time at 0.3 V with 100.0 nM Hg(II). ΔI_p increased significantly with increasing deposition time up to 720 s, but then only slightly, possibly due to saturation. To avoid this saturation at a higher concentration, 600 s was selected as the deposition time for Hg(II) accumulation.

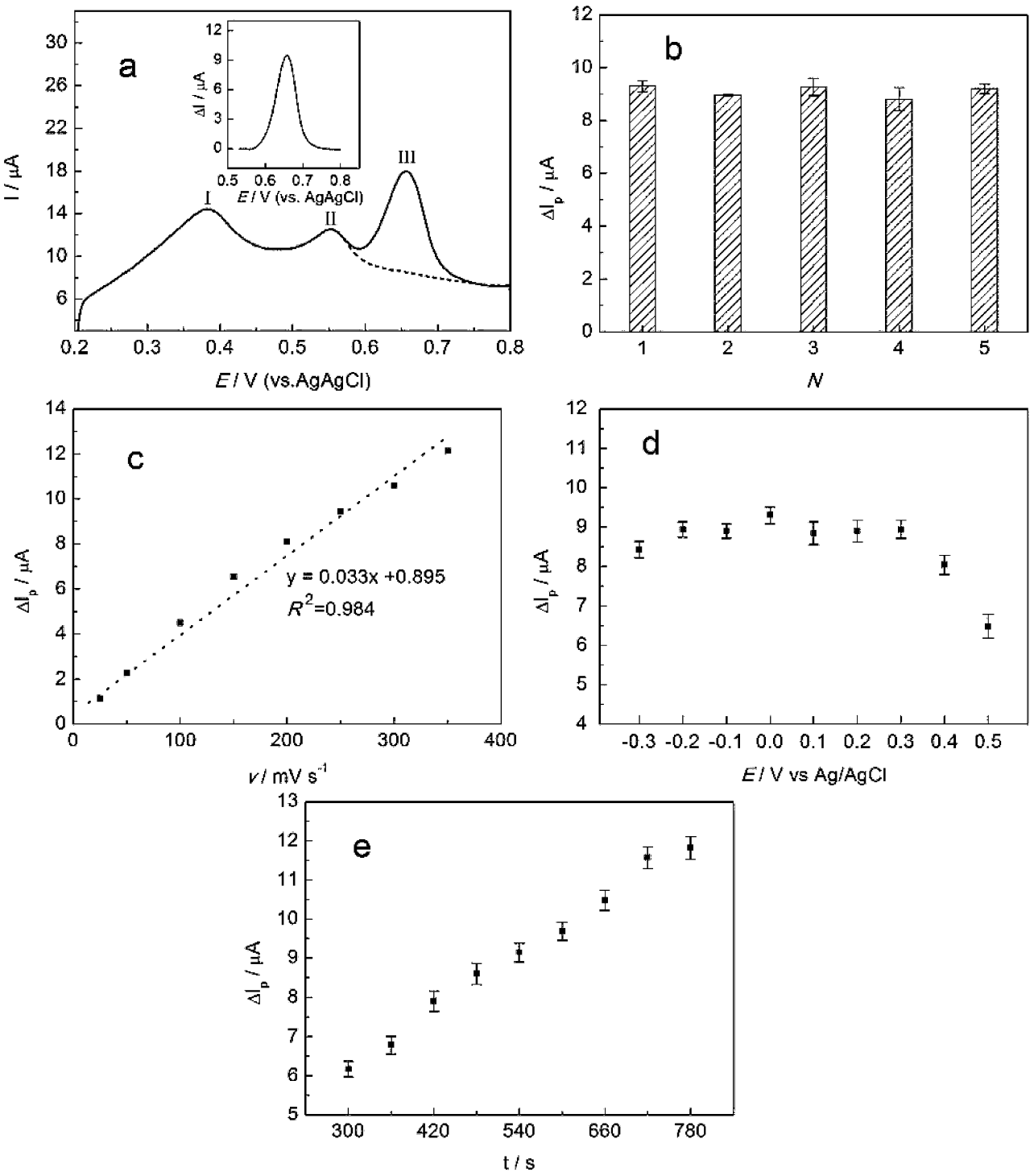

Fig. 5. (a) Stripping voltammograms at a rGO-Au/GCE ($N=1$) in 0.01 M HCl containing 100.0 nM Hg(II) for a deposition time of 600 s (—) and the blank (·····). Inset: Resulting signal after subtraction of the background. Effects of (b) deposition cycles of rGO-Au, (c) scan rate, (d) accumulation potential and (e) accumulation time of Hg(II) on the stripping response of 100.0 nM Hg(II) at rGO-Au/GCE in 0.01 M HCl.

3.5 Analytical Performance for Hg(II) Determination

Using the optimized experimental conditions, the rGO-Au/GCE was applied to the determination of Hg(II). Figure 6 Inset shows the stripping voltammograms at a rGO-Au/GCE over a wide range of concentration (1.0 to 200 nM). As seen in Figure 6, excellent linearity of peak current versus Hg(II) concentration is obtained when the concentration of Hg^{2+} is in the range of 1–150 nM with a sensitivity of $1.12 \pm 0.02\ \mu A\ nM^{-1}\ cm^{-2}$ and

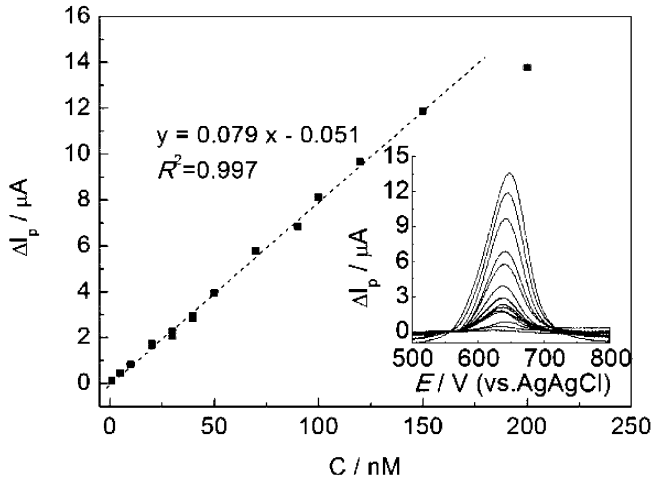

Fig. 6. Calibration curve obtained by stripping voltammetry at a rGO-Au/GCE. Inset: Stripping voltammograms after addition of 1, 5, 10, 20, 30, 40, 50, 70, 90, 100, 120, 150 and 200 nM Hg(II) in 0.01 M HCl.

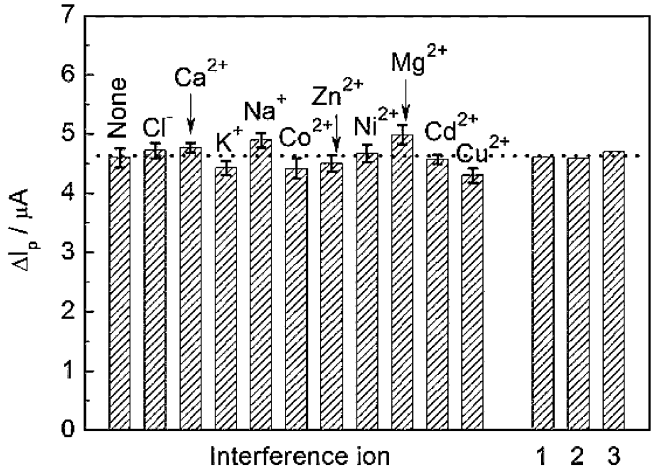

Fig. 7. Effect of other ions on the electrochemical stripping signals of 60 nM Hg(II) at a rGO-Au/GCE. Electrochemical stripping signals (1, 2 and 3) of 60 nM Hg(II) at the same rGO-Au/GCE after the investigation for interference.

a correlation coefficient (R^2) of 0.997. A limit of detection (*LOD*) estimated based the standard 3σ method [43] is 0.6 nM. Thus, the rGO-Au/GCE method exhibits a very wide concentration range for detection of Hg(II) with a very low detection limit and the rGO-Au nanocomposite construct provides a high-performance for Hg(II) detection. Importantly, the detection limit is well below the guideline value for Hg(II) in drinking water (5 nM) [4]. This sensor is among the most sensitive electrochemical Hg(II) sensor reported so far [19,30].

Due to the likely presence of a wide variety of other metal ions in environmentally important samples, selective detection of Hg(II) represents a challenging task. The ions could be co-deposited and stripped off under the experimental condition used for the detection of Hg(II). Possible interferences, arising from Ca^{2+}, Na^+, K^+, Zn^{2+}, Co^{2+}, Ni^{2+}, Mg^{2+}, Cd^{2+}, Cu^{2+} and Cl^-, were investigated to evaluate the selectivity of rGO-Au/GCE to Hg(II). Figure 7 shows the electrochemical stripping signals of mercury in the presence of a 50-fold concentration excess of other elements. The same electrode was used throughout the measurements. The Hg stripping peak current was virtually unaltered, suggesting no interfere of these cations in the detection of Hg(II). This could be inferred from the order of different standard electrode potentials ($E_{M/M}{}^{n+}$) in aqueous solutions [41]. Evidently, the rGO-Au/GCE possesses high selectivity for Hg(II). To confirm the stability and the reusability of the electrode, after the investigation of the effect from other ions, the same rGO-Au/GCE was used for Hg(II) detection in an electrolyte medium containing 60 nM of Hg(II) for 3 consecutive runs. As can be seen from the electrochemical stripping signals (1, 2 and 3, and None) in Figure 7, the rGO-Au/GCE provides excellent reproducibility (relative standard deviation (*RSD*) = 1.5 %). Furthermore, these signals are also comparable to those obtained from the same medium before the investigation of the effect from potentially interfering ions (labeled as "None" in Figure 7). This comparison suggests that the rGO-Au/GCE is stable and reusable, which is a highly attractive feature of this Hg(II) sensor given the fact that gold is a highly precious noble metal.

As the detection limit achieved is well below the guideline value of Hg(II) in drinking water [4], it is expected that rGO-Au/GCE could be used with tap water samples (from Melbourne, Australia) to evaluate the feasibility of application using the standard addition method. The only treatment of the sample was supporting electrolyte addition of 0.01 M HCl. However, Hg(II) was undetectable in these tap water samples. Thus standard solutions were introduced to give an added concentration of 5 nM, 20 nM and 30 nM for quantitative determination, respectively. The stripping analysis was performed under optimized experimental conditions mentioned above and the recoveries are summarized in Table 1.

Table 1. Results for the determination of Hg(II) in the tap water samples using the proposed method (n = 3).

Sample	Hg(II) (nM)		Recovery (%)	*RSD* (%)
	Added	Found		
Tap water 1	5	4.8	96.5	1.8
Tap water 2	20	19.1	95.5	2.6
Tap water 3	30	31.4	104.7	2.3

4 Conclusions

Reduced graphene oxide-gold nanocomposite films have been fabricated via a one-step electrodeposition method and applied for the reusable selective determination of trace Hg(II). Excellent sensitivity (1.12 ± 0.02 μA nM^{-1} cm^{-2}) and low *LOD* (0.6 nM) have been achieved. The sensor should be suitable for the detection

of Hg(II) in environmental monitoring applications. The sensing strategy developed provides an excellent platform for the construction of heavy metal chemical sensors that can be used in aqueous media.

Acknowledgements

This study was financially supported by the *China Scholarship Council*. The authors would like to thank *Monash Microscopy Center* for SEM images and EDX data.

References

[1] R. Tang, Q. Li, L. Ding, H. Cui, J. P. Zhai, *Environ. Technol.* **2012**, *33*, 341.
[2] R. Eisler, *Environ. Geochem. Health* **2003**, *25*, 325.
[3] J. M. Gong, T. Zhou, D. D. Song, L. Z. Zhang, *Sens. Actuators B, Chem.* **2010**, *150*, 491.
[4] *Guidelines for Drinking-Water Quality*, 3rd ed., World Health Organization, Geneva, **2008**, http://www.who.int/water_sanitation_health/dwq/gdwq3rev/en/.
[5] P. Salaun, C. M. G. van den Berg, *Anal. Chem.* **2006**, *78*, 5052.
[6] R. Puk, J. H. Weber, *Anal. Chim. Acta* **1994**, *292*, 175.
[7] M. J. Bloxham, S. J. Hill, P. J. Worsfold, *J. Anal. At. Spectrom.* **1996**, *11*, 511.
[8] H. Xu, L. P. Zeng, S. J. Xing, G. Y. Shi, J. S. Chen, Y. Z. Man, L. T. Jin, *Electrochem. Commun.* **2008**, *10*, 1893.
[9] P. Ugo, S. Zampieri, L. M. Moretto, D. Paolucci, *Anal. Chim. Acta* **2001**, *434*, 291.
[10] L. Hakim, A. Sabarudin, K. Oshita, M. Oshima, S. Motomizu, *Talanta* **2008**, *76*, 1256.
[11] C. Dietz, Y. Madrid, C. Camara, P. Quevauviller, *J. Anal. At. Spectrom.* **1999**, *14*, 1349.
[12] G. M. S. Alves, J. M. C. S. Magalhaes, H. M. V. M. Soares, *Electroanalysis* **2013**, *25*, 493.
[13] W. Yue, B. L. Riehl, N. Pantelic, K. T. Schlueter, J. M. Johnson, R. A. Wilson, X. F. Guo, E. E. King, W. R. Heineman, *Electroanalysis* **2012**, *24*, 1039.
[14] O. Abollino, A. Giacomino, M. Ginepro, M. Malandrino, I. Zelano, *Electroanalysis* **2012**, *24*, 727.
[15] J. Wang, *Analytical Electrochemistry*, 3rd ed., WILEY-VCH, Weinheim **2006**.
[16] J. Wang, *Stripping Analysis: Principles, Instrumentation, and Applications*, 1st ed., VCH, Weinheim **1985**.
[17] X. Dai, G. G. Wildgoose, C. Salter, A. Crossley, R. G. Compton, *Anal. Chem.* **2006**, *78*, 6102.
[18] H. Xu, L. P. Zeng, S. J. Xing, G. Y. Shi, Y. Z. Xian, L. T. Lin, *Electrochem. Commun.* **2008**, *10*, 1839.
[19] O. Abollino, A. Giacomino, M. Malandrino, G. Piscionieri, E. Mentasti, *Electroanalysis* **2008**, *20*, 75.
[20] T. Hezard, K. Fajerwerg, D. Evrard, V. Colliere, P. Behra, P. Gros, *J. Electroanal. Chem.* **2012**, *664*, 46.
[21] T. Hezard, K. Fajerwerg, D. Evrard, V. Collière, P. Behra, P. Gros, *Electrochim. Acta* **2012**, *73*, 15.
[22] L. Ding, J. P. Zhai, A. Bond, J. Zhang, *J. Electroanal. Chem.* **2013**, *704*, 96.
[23] E. Sharon, X. Liu, R. Freeman, O. Yehezkeli, I. Willner, *Electroanalysis* **2013**, *25*, 851.
[24] M. Pumera, *Chem. Soc. Rev.* **2010**, *39*, 4146.
[25] D. A. C. Brownson, C. E. Banks, *Analyst* **2010**, *135*, 2768.
[26] M. Pumera, *Mater. Today* **2011**, *14*, 308.
[27] D. A. C. Brownson, C. W. Foster, C. E. Banks, *Analyst* **2012**, *137*, 1815.
[28] S. Sattayasamitsathit, Y. E. Gu, K. Kaufmann, W. Z. Jia, X. Y. Xiao, M. Rodriguez, S. Minteer, J. Cha, D. B. Burckel, C. M. Wang, R. Polsky, J. Wang, *J. Mater. Chem. A* **2013**, *1*, 1639.
[29] K. H. Chen, G. H. Lu, J. B. Chang, S. Mao, K. H. Yu, S. M. Cui, J. H. Chen, *Anal. Chem.* **2012**, *84*, 4057.
[30] N. Zhou, J. H. Li, H. Chen, C. Y. Liao, L. X. Chen, *Analyst* **2013**, *138*, 1091.
[31] C. B. Liu, K. Wang, S. L. Luo, Y. H. Tang, L. Y. Chen, *Small* **2011**, *7*, 1203.
[32] W. S. Hummers, R. E. Offeman, *J. Am. Chem. Soc.* **1958**, *80*, 1339.
[33] S. X. Guo, S. F. Zhao, A. M. Bond, J. Zhang, *Langmuir* **2012**, *28*, 5275.
[34] L. Chen, Y. Tang, K. Wang, C. Liu, S. Luo, *Electrochem. Commun.* **2011**, *13*, 133.
[35] Z. G. Le, Z. R. Liu, Y. Qian, C. Y. Wang, *Appl. Surf. Sci.* **2012**, *258*, 5348.
[36] G. Goncalves, P. A. A. P. Marques, C. M. Granadeiro, H. I. S. Nogueira, M. K. Singh, J. Gracio, *Chem. Mater.* **2009**, *21*, 4796.
[37] S. J. Guo, S. J. Dong, E. K. Wang, *ACS Nano* **2010**, *4*, 547.
[38] S. H. Kim, G. H. Jeong, D. Choi, S. Yoon, H. B. Jeon, S. M. Lee, S. W. Kim, *J. Colloid Interf. Sci.* **2013**, *389*, 85.
[39] S. Stankovich, D. A. Dikin, R. D. Piner, K. A. Kohlhaas, A. Kleinhammes, Y. Jia, Y. Wu, S. T. Nguyen, R. S. Ruoff, *Carbon* **2007**, *45*, 1558.
[40] T. Hezard, L. Laffont, P. Gros, P. Behra, D. Evrard, *J. Electroanal. Chem.* **2013**, *697*, 28.
[41] A. J. Bard, L. R. Faulkner, *Electrochemical Methods: Fundamentals and Applications*, 2nd ed., Wiley, Hamilton **2001**.
[42] R. Feeney, S. P. Kounaves, *Anal. Chem.* **2000**, *72*, 2222.
[43] D. MacDougall, W. B. Crummett, *Anal. Chem.* **1980**, *52*, 2242.

Received: May 10, 2013
Accepted: June 28, 2013
Published online: September 25, 2013

